DOI: 10.1002/ejic.201001097

Terpyridine Oxovanadium(IV) Complexes of Phenanthroline Bases for Cellular Imaging and Photocytotoxicity in HeLa Cells

Bhabatosh Banik,[a] Pijus K. Sasmal,[a] Sovan Roy,[a] Ritankar Majumdar,[b] Rajan R. Dighe,[b] and Akhil R. Chakravarty*[a]

Keywords: Medicinal chemistry / Vanadium / DNA cleavage / Antitumor agents / Imaging agents / Photodynamic therapy / Cytotoxicity

Oxovanadium(IV) complexes $[VO(N\text{-}N\text{-}N)(N\text{-}N)](NO_3)_2$ (**1**–**4**) of (4′-phenyl)-2,2′:6′,2′′-terpyridine (ph-tpy in **1** and **2**) or (4′-pyrenyl)-2,2′:6′,2′′-terpyridine (py-tpy in **3** and **4**) having N-N as 1,10-phenanthroline (phen in **1** and **3**) or dipyrido[3,2-*a*:2′,3′-*c*]phenazine (dppz in **2** and **4**) are prepared and characterized. The crystal structure of **1** has VO^{2+} group in VN_5O coordination geometry. The terpyridine ligand coordinates in a meridional binding mode. The phen ligand displays a chelating mode of binding with an N-donor site *trans* to the vanadyl oxo group. The complexes show a d-d band in the range of 710–770 nm in aqueous DMF (4:1 v/v). The complexes exhibit an irreversible V^{IV}/V^{III} redox response near –1.0 V vs. SCE in aqueous DMF/0.1 M KCl. The complexes bind to CT DNA giving K_b values within 3.5×10^5 to 1.2×10^6 M^{-1}. The complexes show poor chemical nuclease activity in dark. Complexes **2**–**4** show photonuclease activity in UV-A light of 365 nm forming $^1O_2$ and $^{\cdot}OH$. Complex **4** shows DNA photocleavage activity at near-IR light of 785 nm forming $^{\cdot}OH$ radicals. Complexes **2** and **4** show significant photocytotoxicity in HeLa cancer cells. Uptake of the complexes in HeLa cells, studied by fluorescence imaging, show predominantly cytosolic localization inside the cells.

Introduction

Transition-metal complexes having phenanthroline bases have been extensively used as DNA-cleaving agents,[1–3] DNA structural probes,[4,5] DNA photoprobes,[6] DNA molecular light switches,[7–9] and for other applications.[10–12] Such complexes with their varied coordination environments and versatile redox, spectral and magnetic properties could act as multi-utility model hydrolytic/oxidative nucleases and potential cytotoxic agents.[13–16] Among different applications, the complexes showing photocleavage of DNA and photocytotoxic properties in visible light are of importance as photo-activated chemotherapeutic agents.[17–21] The concept of using metal-based photocytotoxic agents originates from the medicinal use of organic dyes like Photofrin® as photodynamic therapy (PDT) agents that selectively damage cancer cells in red light leaving the unexposed healthy cells unaffected.[22–26] PDT presents a non-invasive treatment modality of cancer as a viable alternative to chemotherapy. The metal-based PDT agents could alleviate problems associated with the porphyrin-based PDT agents that show prolonged skin toxicity and hepatotoxicity.[27,28] The need for metal-based PDT agents also arises to circumvent the toxic effects of the chemotherapeutic drugs like cisplatin and its analogues.[14–21,29,30]

The conventional PDT process requires simultaneous presence of a photosensitizer, molecular oxygen and low-energy light source for the drug activity.[31,32] It selectively brings out apoptosis of the photo-exposed cancer cells, leaving the unexposed normal cells unaffected. Among the large variety of metal complexes used for PDT, lutetium(III) texaphyrin (LUTRIN®) is known to show PDT activity in near-IR light (λ_{max}, 732 nm).[21] Sadler and co-workers have shown that a Pt^{IV} complex with two photo-labile *trans* azide ligands, forms cisplatin analogue on photo-activation and the in situ generated species is cytotoxic towards a variety of cancer cells including those that are resistant to cisplatin.[14] Metal nitrosyl complexes are reported as PDT agents causing cellular damage on photo-release of nitric oxide (NO) at the cancer cells.[16,20] Dirhodium(II) complexes cause oxidative DNA damage in visible light via both oxygen-dependent and independent pathways.[15,21] We have recently reported the photocytotoxicity of oxovanadium(IV) and iron(III) complexes having photoactive dipyridophenazine ligand in visible light.[29,30]

The present work stems from our interest to design and synthesize ternary oxovanadium(IV) complexes having ligand with a fluorophore moiety. The complexes could show efficient photo-induced DNA cleavage activity in near-IR light, low dark cytotoxicity and significant visible light-in-

[a] Department of Inorganic and Physical Chemistry, Indian Institute of Science,
Bangalore 560012, India
Fax: +91-80-23600683
E-mail: arc@ipc.iisc.ernet.in
[b] Department of Molecular Reproduction, Development and Genetics, Indian Institute of Science,
Bangalore 560012, India

Supporting information for this article is available on the WWW under http://dx.doi.org/10.1002/ejic.201001097.

duced photocytotoxicity in cancer cells besides being useful for cellular imaging. We have chosen vanadium metal since this metal plays significant roles in a variety of chemical and biological systems.[33–35] Vanadium is a biologically essential element, encountered in various metalloenzymes such as haloperoxidases[36] or nitrogenases.[37] In addition to this natural relevance, a large variety of biological activities of small vanadium complexes that include enzyme inhibitory,[38] mitogenic[39] or insulin mimetic activities,[40] have been reported. Vanadium compounds are also known to show antitumor effects.[41,42] Bleomycin vanadyl(IV) and $[VO(phen)(H_2O)_2]^{2+}$ are efficient chemical nucleases in the presence of H_2O_2.[43,44] Further, our choice for vanadium(IV) complexes is due to the presence of a low energy absorption band in the PDT spectral window of 630–800 nm. An important aspect of PDT is to design molecules that could cleave DNA at ca. 700 nm considering significant skin penetration of light in the near IR region. We have chosen terpyridine (N-N-N) and phenanthroline base (N-N) as ligands to prepare ternary systems of the type "(N-N-N)-($V^{IV}O$)-(N-N)", where both the planar and photoactive organic ligands could act as DNA binders cum photosensitizers.[45,46] The terpyridine ligand could also render structural stability to the DNA complex adduct since platinum(II) complexes of terpyridine derivatives are reported to show good antitumor activity via stabilazation of G-quadruplex.[47,48] Also, the pyrenyl moiety could serve as "fluorescent tag" for cellular imaging. Herein, we present the synthesis, structure, near-IR light-induced DNA photocleavage and visible light-induced photocytoxic property of four oxovanadium(IV) complexes of formulation $[VO(N\text{-}N\text{-}N)(N\text{-}N)](NO_3)_2$ (**1**–**4**), where "N-N-N" is (4′-phenyl)-2,2′:6′,2′′-terpyridine (ph-tpy in **1** and **2**) or (4′-pyrenyl)-2,2′:6′,2′′-terpyridine (py-tpy in **3** and **4**) and "N-N" is *N*,*N*-donor phenanthroline bases, viz. 1,10-phenanthroline (phen in **1** and **3**) and dipyrido[3,2-*a*:2′,3′-*c*]phenazine (dppz in **2** and **4**) (Scheme 1). The significant result of this study is the PDT effect observed for complex **4** and its use in cellular imaging.

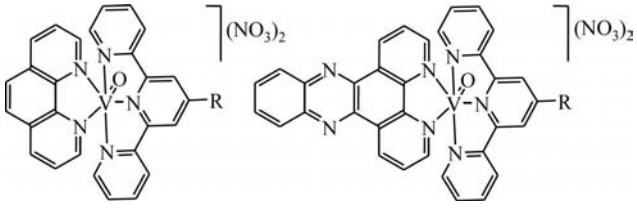

Scheme 1. Oxovanadium(IV) complexes **1**–**4** with R as phenyl (in **1** and **2**) or pyrenyl (in **3** and **4**) group.

Results and Discussion

Synthesis and General Properties

Oxovanadium(IV) complexes of formulations $[VO(ph\text{-}tpy)(N\text{-}N)](NO_3)_2$ (N-N = phen in **1**; dppz in **2**) and $[VO(py\text{-}tpy)(N\text{-}N)](NO_3)_2$ (N-N = phen in **3**; dppz in **4**) were synthesized using a general synthetic procedure in which vanadyl nitrate was treated with the corresponding terpyridine ligand and the phenanthroline base in ethanol. The complexes were characterized from the analytical and spectroscopic data. Selected physicochemical data are given in Table 1. The ESI-MS spectra of the complexes in CH_3CN show essentially the parent ion peak as $[M]^{2+}$ suggesting the solution stability of the complexes. The 1:2 electrolytic complexes are soluble in aqueous DMF giving a molar conductance value of ca. 150 $S\,m^2\,M^{-1}$ in 25% DMF/water. The complexes show characteristic vanadyl (V=O) and nitrate (NO_3^-) infrared bands at ca. 965 and ca. 1385 cm^{-1}, respectively. The complexes are one-electron paramagnetic giving a magnetic moment value of ca. 1.6 μ_B at 25 °C for $3d^1$ electronic configuration. The visible electronic spectra of the complexes **1**–**4** in 25% DMF/water show low-energy low-intensity metal-centered band in the range 710–770 nm (Figure 1). A significant bathochromic shift of the d-d band is observed on changing the pendant group of terpyridine ligand from phenyl to pyrenyl moiety. An intense band observed at ca. 500 nm for the py-tpy complexes could be due to ligand-to-metal charge-transfer transition and the remaining bands appearing in the UV region are assignable to the intraligand transitions.[49] The complexes also show a band at ca. 270 nm assignable to the ligand-based $\pi\rightarrow\pi^*$ transition. The dppz ligand exhibits an additional band near 350 nm assignable to the $n\rightarrow\pi^*$ transition involving the phenazine moiety.[45] The terpyridyl complexes show emission spectral band at 355 nm for **1**; 410, 434 nm for **2**; 408, 461 nm for **3**; and 406, 457 nm for **4** when excitated at 267, 360, 345 and 362 nm, respectively, in

Table 1. Selected physicochemical data for the complexes $[VO(N\text{-}N\text{-}N)(N\text{-}N)](NO_3)_2$.

	IR[a] [cm^{-1}] $\tilde{\nu}$ (NO_3^-)	$\tilde{\nu}$ (V=O)	Electronic[b]: λ_{max} [nm] (ε [$dm^3\,M^{-1}\,cm^{-1}$])	Emission[c] λ_f [nm]	μ_{eff}[d]	Λ_M[e] [$S\,m^2\,M^{-1}$]	E_{pc}[f] [V]	K_b[g] [M^{-1}]	ΔT_m[h] [°C]
1	1387	964	715 (46)	355[i]	1.61	145	–1.00	$3.5(\pm0.6)\times10^5$	3.3
2	1391	969	724 (53)	410, 434[j]	1.63	152	–0.85	$5.4(\pm0.5)\times10^5$	3.7
3	1385	966	776 (34)	408, 461	1.65	150	–0.83	$8.4(\pm0.3)\times10^5$	5.5
4	1382	963	756 (43)	406, 457	1.66	158	–0.85	$1.2(\pm0.2)\times10^6$	7.1

[a] KBr mull. [b] Visible electronic band in 25% DMF/water. [c] Emission spectra of **1**–**4** (10 μM) in aqueous DMSO (1:1 v/v) with λ_{exi} [nm] = 267 (for **1**), 360 (for **2**), 345 (for **3**) and 362 (for **4**). [d] μ_{eff} in μB for solid powdered samples at 298 K. [e] Λ_M, molar conductance in 25% DMF/water at 25 °C. [f] Cathodic peak potential in 25% DMF/water having 0.1 M KCl as supporting electrolyte at 50 mV s^{-1} scan rate. [g] Equilibrium DNA binding constant determined from the UV/Vis absorption titration. [h] Change in the DNA melting temperature. [i] 343 nm (shoulder). [j] 465 nm (shoulder).

50% aqueous DMSO. The emission spectral features are similar to those observed for analogous terpyridyl complexes.[50]

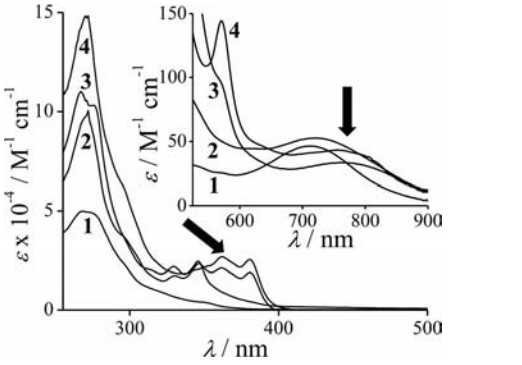

Figure 1. Electronic spectra of the oxovanadium(IV) complexes $[VO(ph\text{-}tpy)(N\text{-}N)](NO_3)_2$ (N-N = phen, **1**; dppz, **2**) and $[VO(py\text{-}tpy)(N\text{-}N)](NO_3)_2$ (N-N = phen, **3**; dppz, **4**) in 25% DMF/water. The inset shows the d-d band. The wavelengths used for DNA photocleavage studies are shown by arrows.

Complexes **1**–**4** are redox-active showing cyclic voltammetric responses involving the metal center, terpyridine ligands and the phenanthroline bases in 25% DMF –0.1 M KCl (Table 1). The complexes do not show any oxidative response indicating stability of the complexes towards oxidizing agents. The complexes display an irreversible voltammetric response in the potential range –0.8 to –1.0 V vs. S.C.E. This redox process is assignable to the V^{IV}/V^{III} couple. All the complexes exhibit ligand-based reductions. While the phen complexes display an irreversible reduction near –1.2 V, the dppz complexes show ligand-based quasi-reversible redox process in the range –1.1 to –1.2 V, respectively. The complexes also show terpyridine-based reductive response in the range of –1.5 to –1.8 V.

The phen complex of the ph-tpy ligand as **1**·1.5ClO_4·0.5PF_6·CH_3CN was structurally characterized by single-crystal X-ray diffraction technique. An ORTEP view of the cationic complex is shown in Figure 2. The structure of the complex consists of a discrete monomeric vanadium(IV) species with a VO^{2+} moiety bonded to a 4′-phenyl-2,2′:6′,2′′-terpyridine ligand and a *N*,*N*-donor phenanthroline base (phen). The terpyridine ligand is bonded through the nitrogen atoms of the pyridyl groups. The complex has $V^{IV}N_5O$ coordination geometry. The V=O distance is ca. 1.6 Å. The terpyridine ligand displays meridional mode of binding to the metal centre. The phenanthroline base binds at the axial-equatorial positions. The V–N bond *trans* to the V=O group is significantly long compared to the other V–N distances. The coordination geometry is significantly distorted from the octahedral structure. The structure of the complex shows that the DNA binding moieties are not sterically encumbered.

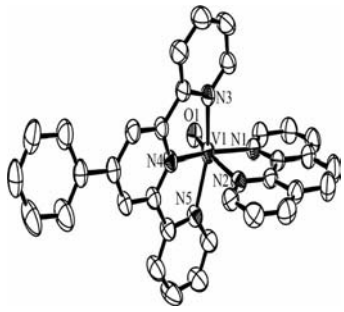

Figure 2. An ORTEP view of the cationic complex in [VO(ph-tpy)(phen)]·1.5ClO_4·0.5PF_6·CH_3CN (**1**·1.5ClO_4·0.5PF_6·CH_3CN) showing atom labelling Scheme for the metal and hetero atoms and 50% probability thermal ellipsoids. The hydrogen atoms are not shown for clarity.

DNA Binding Properties

Absorption titration method was used to monitor the interaction of the complexes **1**–**4** with CT DNA. Intercalation of a complex to DNA generally results in hypochromism and red shift (bathochromism) of the absorption band due to strong stacking interaction between the aromatic chromophore of the ligand and the base pairs of the DNA.[51] The extent of hypochromism thus gives an estimate of the strength of an intercalative binding. The observed trend in hypochromism among the present vanadyl complexes follows the order: **4** > **3** > **2** > **1**. The intrinsic equilibrium DNA binding constant (K_b) values of the complexes follow the same order as observed in the trend of hypochromism (Table 1). The observed difference could be related to the DNA binding preference of the terpyridine ligands as well as that of the phenanthroline bases. The dppz ligand with an extended aromatic moiety is a better binder to DNA than the phen ligand.[7] The binding constant value of the dppz complex having py-tpy ligand is similar to that of the DNA intercalator ethidium bromide.

Thermal behaviour of DNA in the presence of metal complexes can give insight into their conformational changes and about the interaction strength of the complexes with DNA when temperature is raised. The double-stranded DNA gradually dissociates to single strands on increasing the solution temperature and generates a hyperchromic effect on the absorption spectra of the DNA bases (λ_{max} = 260 nm). In order to identify this transition process, the melting temperature T_m, which is defined as the temperature where half of the total base pairs gets non-bonded, is an important parameter. An increase in the DNA melting temperature (ΔT_m) is observed on addition of the complexes to CT DNA (Table 1, Figure 3). Complex **4** shows a high melting temperature which is comparable to that of the ethidium bromide. The ΔT_m values suggest partial intercalation of the complexes to CT DNA stabilizing the DNA double helix structure in preference to the electrostatic mode of binding to DNA that normally gives small positive values of ΔT_m.[52–55] The intercalative mode of DNA binding could be due to the presence of planar terpyridine and phenanthroline ligands in the complexes. The py-tpy complexes **3** and **4** show higher ΔT_m values than their ph-tpy analogues **1** and **2**. This could possibly be due to larger aromatic moiety in the pyrenyl group in comparison to the phenyl group.

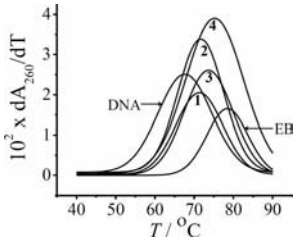

Figure 3. Thermal denaturation plots of 150 μM CT DNA alone and in the presence of [VO(ph-tpy)(N-N)]$(NO_3)_2$ (N-N = phen, **1**; dppz, **2**) and [VO(py-tpy)(N-N)]$(NO_3)_2$ (N-N = phen, **3**; dppz, **4**) and ethidium bromide (EB) at 37.0(±0.1) °C in 5 mM phosphate buffer (pH 6.85) with a [DNA]/[complex] ratio of 10:1.

Viscosity measurements are done to examine the effect on the specific relative viscosity of CT DNA upon addition of the oxovanadium(IV) complexes. Since the relative specific viscosity (η/η_0) of DNA gives a measure on the increase in contour length associated with the separation of DNA base pairs due to intercalation, a DNA intercalator like EB shows significant increase in the viscosity of the DNA solutions (η and η_0 are the specific viscosities of DNA in the presence and absence of the complexes, respectively).[55–58] The plot of relative specific viscosity $(\eta/\eta_0)^{1/3}$ vs. [complex]/[DNA] ratio for the present complexes shows major change in the viscosity for all the complexes. Complex **4** having py-tpy and dppz ligand shows similar $(\eta/\eta_0)^{1/3}$ values like EB, indicating intercalative nature of DNA binding of this complex. The binding nature follows an order of the (η/η_0) values as **4** > **3** > **2** > **1** (Figure 4). The DNA groove binder Hoechst 33258 is used as a control. The viscosity data suggest intercalative binding propensity of complexes to DNA.

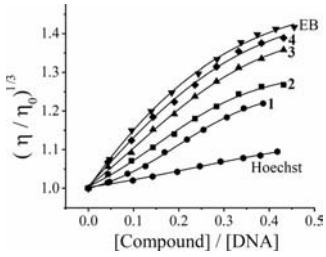

Figure 4. Plots showing the effect of addition of an increasing quantity of the complexes and the control compounds on the relative viscosity of CT DNA (140 μM) at 37.0(±0.1) °C in the presence of **1**–**4**, DNA intercalator ethidium bromide (EB) and DNA groove binder Hoechst 33258.

Chemical Nuclease Activity

The cleavage of SC pUC19 DNA (30 μM) by **1**–**4** (50 μM) in Tris-HCl/NaCl medium was studied in dark using 3-mercaptopropionic acid (MPA, 0.5 mM) and glutathione (GSH, 0.5 mM) as reducing agents. The complexes alone did not show any apparent DNA cleavage in dark suggesting inactivity of the complexes towards hydrolytic cleavage of DNA. The complexes were also found to be cleavage inactive in the presence of both MPA and GSH. The lack of chemical nuclease activity could presumably be due to high negative redox potential values of the $\{V^{IV}O\}^{2+}/\{V^{III}O\}^{+}$ couple. In contrast, oxo-bridged divanadium(III) complexes having 1,10-phenanthroline base are known to show significant chemical nuclease activity cleaving plasmid DNA via hydroxy or superoxide radical pathway.[59] Similarly, bleomycin-vanadyl(IV) and $[VO(phen)(H_2O)]^{2+}$ complexes oxidatively cleave DNA in the presence of hydrogen peroxide.[43,44] The poor chemical nuclease activity of the present complexes is a significant result since the complexes are expected to show less dark cytotoxicity, while being photocytotoxic in visible light.

DNA Photocleavage Study

The photo-induced DNA cleavage activity of the complexes was studied using SC pUC19 DNA in a medium of Tris-HCl/NaCl buffer on irradiation with monochromatic UV-A light of 365 nm and near-IR light of 785 nm using a diode laser (Figure 5). Complex **1** having ph-tpy and phen ligands showed only moderate DNA cleavage activity at these wavelengths in absence of an efficient photosensitizer. Complexes **2**–**4** having photoactive ligand(s) are efficient photocleavers of DNA. A 20 μM solution of **2**–**4** shows essentially complete cleavage of SC DNA to its nicked circular (NC) form on 1.0 h photoexposure in UV-A light of 365 nm. Control experiments with only SC DNA at this wavelength or SC DNA in the presence of **4** in dark did not show any significant DNA cleavage activity. The ligands alone were cleavage inactive under similar reaction conditions. The DNA binding property of the complexes was further explored using DNA minor groove binder distamycin-A. Distamycin-A (50 μM) alone showed ca. 14% cleavage of SC DNA (30 μM) to its NC form at 365 nm for 1.0 h exposure time. Addition of complex **1** to the distamycin-bound SC DNA showed significant inhibition in the DNA cleavage activity, while no such inhibition was observed for the complexes **2**–**4**. The binding of the complexes have also been investigated in presence of DNA major groove binder methyl green. Methyl green (25 μM) alone showed ca. 24% cleavage of SC DNA (30 μM) to its NC form at 365 nm for 1.0 h photoexposure time. Complexes **2**–**4** showed moderate

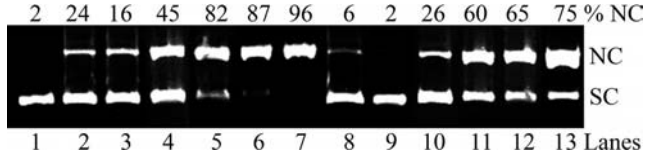

Figure 5. Cleavage of SC pUC19 DNA (0.2 μg, 30 μM) by [VO(ph-tpy)(N-N)]$(NO_3)_2$ (N-N = phen, **1**; dppz, **2**) and [VO(py-tpy)(N-N)]$(NO_3)_2$ (N-N = phen, **3**; dppz, **4**) and ligands in 50 mM Tris-HCl/NaCl buffer (pH 7.2) containing 10% DMF on photo-irradiation with UV-A light of 365 nm (1 h exposure) and near-IR light of 785 nm (2 h exposure) [lanes 1–7 are in UV-A light; lanes 9–13 are in near-IR light]: lane 1, DNA control; lane 2, DNA + py-tpy (20 μM); lane 3, DNA + dppz (20 μM); lanes 4–7, DNA + **1**–**4** (20 μM), respectively; lane 8, DNA + **4** (50 μM, in dark); lane 9, DNA control; lanes 10–13, DNA + **1**–**4** (50 μM) respectively. SC and NC are the supercoiled and nicked circular form of pUC19 DNA.

inhibition in the DNA cleavage activity for methyl green bound SC DNA. The results show that the complexes barring **1** intercalate to SC DNA through the major groove.

The photo-induced DNA cleavage activity of the complexes in near-IR light of 785 nm was studied using 50 μM complex concentration (Figure 5). The choice of this wavelength is based on the presence of a d-d band near 750 nm in the electronic spectra. Complexes **2**–**4** showed significant cleavage of DNA from its SC to NC form at this wavelength. The photo-excitation of the metal complexes seems to be metal-assisted and involves the metal-based charge transfer and d-d bands resulting in an excited state that could generate DNA cleavage active species. Although there is a report on vanadium(V) complexes showing photocleavage of DNA in UV light,[60] observation of DNA cleavage in near-IR light is known for only vanadium(IV) complexes due to the presence of a low-energy visible band.

Mechanistic Studies

DNA cleavage reactions were carried out in the presence of different additives to understand the mechanistic pathways involved in UV-A light and near-IR light (Figure 6). The complexes are cleavage inactive at 365 nm under argon atmosphere. This indicates the necessity of molecular oxygen for the DNA cleavage. The reactions involving molecular oxygen ($^3O_2$) could proceed via two major mechanistic pathways. The excited electronic state of the complex through efficient intersystem crossing could generate an excited state that can activate molecular oxygen to its reactive singlet ($^1O_2$, $^1\Delta_g$) state by a type-II process.[32] In an alternate pathway, the redox active photo-activated complex could reduce molecular oxygen to generate reactive hydroxy radical species by a photo-redox mechanism.[31] We have observed significant inhibition of the photo-induced DNA cleavage activity of the complexes on addition of both singlet oxygen quenchers like sodium azide, TEMP and DABCO and hydroxy radical scavengers like DMSO, KI and catalase to SC DNA. The results suggest the involvement of both singlet oxygen and hydroxy radicals in the photocleavage reactions in UV-A light of 365 nm. The formation of singlet oxygen has further been confirmed from the reaction in presence of D_2O which shows significant enhancement of the cleavage activity due to longer lifetime of $^1O_2$ in this solvent.[61,62] Superoxide dismutase (SOD) showed only marginal inhibition of the cleavage activity.

The photo-induced DNA cleavage reactions in the presence of additives at near-IR wavelength of 785 nm showed only the hydroxy radical photo-redox pathway. Singlet oxygen quenchers showed no inhibitory effect in red light. The hydroxy radical scavengers, however, showed inhibition in the DNA cleavage activity. The photo-activated oxovanadium(IV) species in near-IR light could reduce the metal forming reactive V^{III} species that may lead to the formation of hydroxy radicals following a Fenton-like mechanism which is known for copper-dipyridoquinoxaline and iron-bleomycin species.[63–65] The DNA cleavage reaction in UV-A light of 365 nm is likely to involve the photoactive ligands having phenazine (in dppz) or pyrenyl (in py-tpy) moiety to facilitate the singlet oxygen pathway.

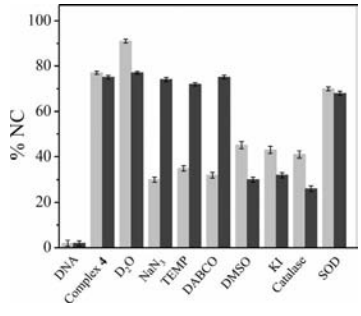

Figure 6. Bar diagram showing the photocleavage of SC pUC19 DNA (0.2 μg, 30 μM) by $[VO(py\text{-}tpy)(dppz)](NO_3)_2$ (**4**) at 365 nm (15 μM, light gray shade) and 785 nm (50 μM, dark gray shade) in the presence of different additives for 2 h exposure time in 50 mM Tris-HCl/NaCl buffer (pH 7.2) [NaN_3, TEMP, DABCO and KI = 500 μM; D_2O, 16 μL; DMSO, 6 μL; catalase, 4 units; SOD, 4 units].

Cytotoxicity Assay

The photocytotoxic property of the complexes **1**–**4** was explored using MTT assay, which is based on the reduction of yellow MTT to purple formazan by mitochondrial reductases of viable cells. The HeLa cells upon 3.0 h incubation with the complexes, followed by photoexposure with broad-band visible radiation (400–700 nm, 10 J cm^{-2}), showed a sigmoidal dose-response inhibition of cell viability. Interestingly, only the dppz complexes **2** and **4** showed photocytotoxicity with IC_{50} values of 26.0 (±1.1) μM and 13.7 (±1.0) μM, respectively (Figure 7). The corresponding phen complexes (**1** and **3**) did not show any significant photocytotoxic activity. Also, the cells treated with the complexes but unexposed to light did not exhibit any significant reduction in cell viability giving IC_{50} values of > 100 μM. Hence, the dppz complexes are only found to be cytotoxic upon visible light irradiation and the dppz ligand seems to have a definite role, possibly in the internalization of the

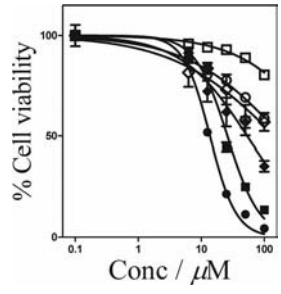

Figure 7. Photocytotoxicity of $[VO(ph\text{-}tpy)(dppz)](NO_3)_2$ (**2**), $[VO(py\text{-}tpy)(dppz)](NO_3)_2$ (**4**) and dppz ligand in human cervical cancer HeLa cells on 3 h incubation in dark followed by photoirradiation in visible light (400–700 nm) as determined by MTT assay. Symbols used for photo-exposed cells: dots for **4**, filled squares for **2**, filled diamonds for dppz; symbols for dark-treated cells: open circles for **4**, open squares for **2**, open diamonds for dppz). The error bars represent the standard deviation of three replicates.

complexes inside the cells. The dppz ligand alone gave an IC_{50} value of 60.1(±2.3) μM in visible light, whereas it did not show any apparent cytotoxicity in HeLa cells in dark. The terpyridine ligand or $VOSO_4$ did not show any reduction in cell viability in dark or upon irradiation with visible light under same reaction conditions. Complex **4** gave lower IC_{50} value than cisplatin (IC_{50} = 70 μM) and showed similar PDT effect as is known for Photofrin® (IC_{50} = 2.57 μM) (Table 2).[66,67] The photocytotoxic property of complex **4** makes it a potential candidate for further study to augment its PDT activity. The effectiveness of **2** and **4** towards showing reduced cell viability was assessed from the statistical analysis.[68]

Table 2. A comparison of the IC_{50} values of the complexes **1**–**4**, ligands and related compounds in HeLa cells.

Compound	IC_{50} [μM] (in visible light)	IC_{50} [μM] (in dark)
$[VO(ph\text{-}tpy)(phen)](NO_3)_2$ (**1**)	> 100	> 100
$[VO(ph\text{-}tpy)(dppz)](NO_3)_2$ (**2**)	26.0	> 100
$[VO(py\text{-}tpy)(phen)](NO_3)_2$ (**3**)	79.3	> 100
$[VO(py\text{-}tpy)(dppz)](NO_3)_2$ (**4**)	13.7	> 100
ph-tpy	> 100	> 100
py-tpy	> 100	> 100
dppz	60.1	> 100
$VOSO_4$	> 100	> 100
$[VOCl(dppz)_2]Cl$[a]	12	> 100
$[Fe(L')(dppz)]$[b]	3.59	> 100
Photofrin®[c]	2.57	> 25
Cisplatin[d][e]	–	7.2

[a] The IC_{50} values are from ref. [29]. [b] The IC_{50} values are from ref. 30 (L′ is a trianionic tetradentate phenolate-based ligand). [c] Photofrin IC_{50} values are from ref. [67]. [d] The cisplatin IC_{50} value for 24 h incubation time was taken from ref. [66]. [e] IC_{50} value of cisplatin for 4 h incubation is 70 μM in dark. There is no apparent effect of visible light on the IC_{50} value of cisplatin.

DAPI Staining

The cellular inhibitory effect of the dppz complexes in HeLa cells has been studied using nuclear staining with DAPI. Complex **4** (15 μM) showed characteristic apoptotic features such as condensed and fragmented chromatin (Figure 8). Therefore, photo-irradiation with complex **4** in visible light (400–700 nm) causes cellular damage leading to cell death.

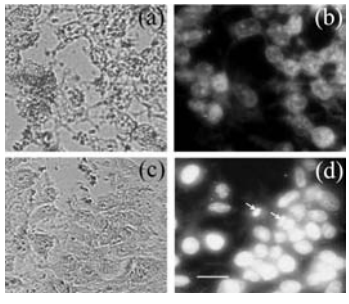

Figure 8. DAPI staining of HeLa cells showing untreated [panels (a), (b)] and treated with complex **4** [panels (c), (d)] on 2 h post photo-exposure to visible light (400–700 nm, 10 J cm^{-2}). The condensed nuclei are shown by arrows and the scale bar corresponds to 20 μm. Panels (b) and (d) are from a fluorescence microscope with 360/40 nm excitation filter and 460/50 nm emission filter. Panels (a) and (c) are their respective bright-field images.

Fluorescence Imaging

To explore the cellular uptake of the complexes and the ligands, fluorescence imaging was carried out using HeLa cells. The HeLa cells on incubation with py-tpy and the complex **4** for 4.0 h showed better uptake for the complex than the corresponding ligands (Figure 9). This behavior of complex **4** may be attributed to the hydrophobicity of the py-tpy and dppz ligands. The localization of the complex inside the HeLa cells is found to be predominantly cytosolic with lesser accumulation in the nucleus. The ligands show similar type of localization in the HeLa cells, but the extent of fluorescence is much less as compared to their corresponding complexes.

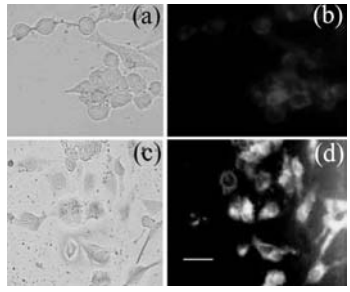

Figure 9. Fluorescence imaging of HeLa cells showing the cellular uptake upon incubation with py-tpy ligand [panels (a) and (b)] and $[VO(py\text{-}tpy)(dppz)](NO_3)_2$ (**4**) [panels (c) and (d)]. The images were recorded with a fixed exposure time and gain for both the fluorescence and bright field modes. Panels (a) and (c) are the bright-field images. Panels (b) and (d) are their respective fluorescence images. The scale bar corresponds to 25 μm.

The results are consistent with the photocytotoxicity data that show lower activity of the ligands as compared to those of the corresponding complexes. This effect is further augmented by the absence of suitable absorption bands in the visible region for the ligands. Complex **4** having the fluorescent pyrene pendant moiety show significant cellular uptake as revealed from the fluorescence intensity inside the HeLa cells. Hence, the higher cellular activity of complex **4** over complex **2**, as observed in the photocytotoxicity assay, seems to be due to better photosensitizing ability of the pyrenyl moiety in py-tpy than the phenyl group in ph-tpy.

Conclusions

We report here water soluble oxovanadium(IV) complexes of terpyridine ligands having pendant phenyl and pyrenyl moieties and planar phenanthroline bases showing efficient DNA binding propensity, visible light-induced DNA cleavage activity and photocytotoxicity. The pyrenyl complexes are used for cellular imaging. Complexes **2**–**4** show efficient photo-induced DNA cleavage activity in near-IR light of 785 nm via formation of hydroxy radicals. The re-

sults are of significance since compounds showing DNA cleavage activity near 800 nm wavelength are virtually unknown in the literature. Complexes **2** and **4** also prove to be significantly effective in reducing the viability of HeLa cells upon visible light irradiation, while they are non-toxic in absence of light. Further, complex **4** having a pendant pyrene moiety has been used for cellular imaging. The fluorescence microscopy studies show the accumulation of the complex inside the cell primarily in the cytosol and to a lesser extent inside the nucleus. It can also be ascertained from the fluorescence intensity that the complexes are able to cross the cellular membrane and get accumulated inside the cell in greater quantities as compared to the ligands alone. Considering bio-essential nature of the metal, the presence of a low-energy visible band within the PDT spectral window and redox activity of the complexes, the results obtained from the present oxovanadium(IV) complexes are of importance towards developing metal-based agents for cellular imaging and PDT applications.

Experimental Section

General: All reagents and chemicals were procured from commercial sources (s.d. Fine Chemicals, India; Aldrich–Sigma, USA) and used without further purifications. Solvents used were purified by standard procedures.[69] Synthesis of the complexes was done under nitrogen atmosphere using Schlenk technique. Supercoiled (SC) pUC19 DNA (cesium chloride purified) was purchased from Bangalore Genie (India). Tris(hydroxymethyl)aminomethane–HCl (Tris-HCl) buffer solution was prepared using deionized and sonicated triple distilled water. Calf thymus (CT) DNA, agarose (molecular biology grade), distamycin-A, methyl green, catalase, superoxide dismutase (SOD), 2,2,6,6-tetramethyl-4-piperidone (TEMP), 1,4-diazabicyclo[2.2.2]octane (DABCO), ethidium bromide (EB), Hoechst 33258 (bis-benzimidazole derivative) were from Sigma (USA). The *N*,*N*-donor heterocyclic base dipyrido[3,2-*a*:2′,3′-*c*]-phenazine (dppz) was prepared by literature procedure using 1,10-phenanthroline-5,6-dione as a precursor reacted with 1,2-phenylenediamine.[70,71] The terpyridine ligands, viz. (4′-phenyl)-2,2′:6′,2′′-terpyridine (ph-tpy) and (4′-pyrenyl)-2,2′:6′,2′′-terpyridine (py-tpy), were prepared by reported procedures.[72–74]

The elemental analysis was done using a Thermo Finnigan Flash EA 1112 CHNS analyzer. The infrared and electronic spectra were recorded on Perkin–Elmer Lambda 35 and Perkin–Elmer Spectrum one 55 spectrophotometers, respectively. Molar conductivity measurements were performed using a Control Dynamics (India) conductivity meter. Room temperature magnetic susceptibility data were obtained from a George Associates Inc. Lewis-coil force magnetometer using $Hg[Co(NCS)_4]$ as a standard. Experimental susceptibility data were corrected for diamagnetic contributions.[75] Cyclic voltammetric measurements were made at 25 °C on a EG& G PAR Model 253 VersaStat potentiostat/galvanostat with electrochemical analysis software 270 using a three electrode set-up comprising of a glassy carbon working, platinum wire auxiliary and a saturated calomel electrode (SCE) as reference. Potassium chloride (KCl, 0.1 M) was used as a supporting electrolyte in 25% DMF/H_2O. The electrochemical data were uncorrected for junction potentials. Electrospray ionization mass spectral measurements were done using Esquire 3000 plus ESI (Bruker Daltonics) and Q-TOF Mass Spectrometer. Fluorescence microscopic investigations were carried out on Leica DM IL microscope with integrated Leica DFC400 camera and IL50 image software.

Preparation of $[VO(ph\text{-}tpy)(N\text{-}N)](NO_3)_2$ (N-N = phen, 1; dppz, 2) and $[VO(py\text{-}tpy)(N\text{-}N)](NO_3)_2$ (N-N = phen, 3; dppz, 4): Oxovanadium(IV) sulfate (0.16 g, 1.0 mmol) was dissolved in 15 mL of EtOH. To this solution was added $Ba(NO_3)_2$ (0.31 g, 1.0 mmol) and the mixture was stirred at an ambient temperature for 2 h. The precipitated barium sulfate was filtered off using celite. The blue filtrate was deaerated and then saturated with nitrogen. An ethanolic solution (15 mL) of the corresponding phenanthroline base [0.20 g, phen; 0.29 g, dppz, (1.0 mmol)] was added to the filtrate. A light-greenish solution was obtained after stirring the mixture for 15 min. To this mixture was added the corresponding terpyridine ligand [0.31 g, ph-tpy; 0.43 g, py-tpy (1.0 mmol)]. The complex was precipitated out on addition of the terpyridine ligand. The precipitate was filtered, isolated and washed with cold EtOH and THF and finally dried in vacuo over P_4O_{10}. The product was recrystallized from MeCN.

$[VO(ph\text{-}tpy)(phen)](NO_3)_2$ (1): Yield 0.54 g, 80%. $C_{33}H_{23}N_7O_7V$ (680.53): calcd. C 58.24, H 3.41, N 14.41; found C 58.15, H 3.12, N 14.22. ESI-MS in MeCN: *m*/*z* 278.73 $[M]^{2+}$. IR (KBr): $\tilde{\nu}$ = 3969 br, 3077 br, 2902 m, 1689 m, 1521 m, 1387 vs (NO_3^-), 964 s (V=O), 902 w, 852 w, 710 w cm^{-1}. UV/Vis, 25% DMF/water {λ_{max} [nm] (ε [$dm^3 M^{-1} cm^{-1}$])}: 715 (46), 276 sh (48660), 267 (49440).

$[VO(ph\text{-}tpy)(dppz)](NO_3)_2$ (2): Yield 0.66 g, 85%. $C_{39}H_{25}N_9O_7V$ (782.62): calcd. C 59.85, H 3.22, N 16.11; found C 59.58, H 2.99, N 16.40. ESI-MS in MeCN: *m*/*z* 330 $[M]^{2+}$. IR (KBr): $\tilde{\nu}$ = 3728 br, 3045 br, 2766 m, 1601 m, 1501 s, 1391 vs (NO_3^-), 969 s (V=O), 825 w, 766 m, 732 m cm^{-1}. UV/Vis, 25% DMF/water {λ_{max} [nm] (ε [$dm^3 M^{-1} cm^{-1}$])}: 724 (53), 380 (19210), 360 (21540), 346 (23100), 330 (20300), 296 sh (37400), 271 (98270).

$[VO(py\text{-}tpy)(phen)](NO_3)_2$ (3): Yield 0.64 g, 78%. $C_{43}H_{27}N_7O_7V$ (804.67): calcd. C 64.18, H 3.38, N 12.18; found C 64.02, H 3.27, N 11.97. ESI-MS in MeCN: *m*/*z* 340 $[M]^{2+}$. IR (KBr): $\tilde{\nu}$ = 3696 br, 3024 br, 2873 m, 1579 m, 1520 m, 1385 vs (NO_3^-), 966 s (V=O), 847 m, 713 w cm^{-1}. UV/Vis, 25% DMF/water {λ_{max} [nm] (ε [$dm^3 M^{-1} cm^{-1}$])}: 776 (34), 569 sh (96), 345 (24660), 329 (22450), 276 sh (102940), 266 (110060).

$[VO(py\text{-}tpy)(dppz)](NO_3)_2$ (4): Yield 0.74 g, 82%. $C_{49}H_{29}N_9O_7V$ (906.77): calcd. C 64.90, H 3.22, N 13.90; found C 64.72, H 3.11, N 14.01. ESI-MS in MeCN: *m*/*z* 391.47 $[M]^{2+}$. IR (KBr): $\tilde{\nu}$ = 3742 br, 3033 br, 2776 m, 1578 w 1492 m, 1382 vs (NO_3^-), 963 s (V=O), 832 w, 771 w cm^{-1}. UV/Vis, 25% DMF/water {λ_{max} [nm] (ε [$dm^3 M^{-1} cm^{-1}$])}: 756 (43), 570 (144), 380 (25800), 362 (26950), 351 sh (21910), 295 sh (62470), 271 (148280).

Solubility and Stability: The complexes showed good solubility in DMF, DMSO, MeCN; moderate solubility in water, methanol, ethanol and poor solubility in hydrocarbons. The complexes showed stability in the solid and solution phases. The complexes were soluble in aqueous DMF.

X-ray Crystallographic Procedures: Complex **1** was crystallized from an CH_3CN solution having $NaClO_4$ and NH_4PF_6 salts. The crystal structure of the perchorate/hexafluorophosphate salt of the complex of formulation $\mathbf{1}\cdot 1.5ClO_4\cdot 0.5PF_6\cdot CH_3CN$ was obtained by single-crystal X-ray diffraction technique. Crystal mounting was done on glass fibre with epoxy cement. All geometric and intensity data were collected at room temperature using an automated Bruker SMART APEX CCD diffractometer equipped with a fine focus 1.75 kW sealed tube Mo-K_α X-ray source (λ = 0.71073 Å) with increasing ω (width of 0.3° per frame) at a scan speed of 2 s per frame. Intensity data, collected using an ω-2θ scan mode, were

corrected for Lorentz polarization effects and for absorption.[76] The structure was solved by the combination of Patterson and Fourier techniques and refined by full-matrix least-squares method using SHELX system of programs.[77] Hydrogen atoms belonging to the complex were in their calculated positions and refined using a riding model. All non-hydrogen atoms were refined anisotropically. While one perchorate anion was refined well with a site-occupancy of one, the other anion was found to be positionally disordered with half ClO_4 and half PF_6 ions. There was one CH_3CN as lattice solvent molecule in the crystallographic asymmetric unit. The disordered atoms were refined isotropically. Selected crystallographic data are given in Table 3. The residual R value is ca. 7% which is within the acceptable range. The structure for the cationic species is found to be of good quality. The positional disorders observed for the lattice anions do not have any apparent effect on the bonding parameters of the cationic complex. The anion disorder may have some effect on the overall quality of the structure but, as far as the cationic species is concerned, the bonding parameters are found to be of good quality. The goodness-of-fit value is 1.03 in absence of any restraints. The largest peak in the DF map is 0.9 e Å^{-3}. A perspective view of the complex was obtained by ORTEP.[78]

Table 3. Selected crystallographic data for [VO(ph-tpy)(phen)]·1.5ClO_4·0.5PF_6·CH_3CN (**1**·1.5ClO_4·0.5PF_6·CH_3CN).

Formula	$C_{35}H_{26}N_6Cl_{1.50}F_3O_7P_{0.50}V$
Crystal size /mm^3	0.35 × 0.32 × 0.29
Fw /g M^{-1}	819.22
Crystal system	triclinic
Space group (no.)	$P\bar{1}$ (2)
a /Å	8.7921(6)
b /Å	12.1906(9)
c /Å	17.3616(12)
α /°	84.505(4)
β /°	75.348(3)
γ /°	79.545(4)
V /Å^3	1768.0(2)
Z	2
T /K	293(2)
ρ_{calc} /g cm^{-3}	1.539
λ /Å (Mo-K_α)	0.71073
μ /mm^{-1}	0.491
F(000)	834
Reflections collected	35888
Unique reflections	10474
Reflections with $I > 2\sigma(I)$	6760
parameters/restraints	380/0
Goodness-of-fit on F^2	1.032
R (F_o)[a] [$I > 2\sigma(I)$]	0.0771
wR (F_o)[b] [$I > 2\sigma(I)$]	0.2315
R [all data] (wR [all data])	0.1127 (0.2688)
Largest difference in peak and hole /e Å^{-3}	0.895, –0.936
$w = [\sigma^2(F_o)^2 + (AP)^2 + (BP)]^{-1}$	A = 0.1584, B = 0.9665

[a] $R = \Sigma||F_o| - |F_c||/\Sigma|F_o|$. [b] $wR = \{\Sigma[w(F_o^2 - F_c^2)^2]/\Sigma[w(F_o)^2]\}^{1/2}$; $w = [\sigma 2(F_o)^2 + (AP)^2 + BP]^{-1}$; where $P = (F_o^2 + 2F_c^2)/3$.

CCDC-793516 contains the supplementary crystallographic data for this paper. These data can be obtained free of charge from The Cambridge Crystallographic Data Centre via www.ccdc.cam.ac.uk/data_request/cif.

DNA Binding Experiments: Interaction studies of the complexes with DNA were carried out in Tris-HCl buffer (50 mM Tris-HCl, pH 7.2) at room temperature. A solution of calf thymus DNA in the buffer gave a ratio of UV absorbance at 260 and 280 nm of about 1.89:1, indicating the DNA sufficiently free from protein. The DNA concentration per nucleotide was determined by absorption spectroscopy using the molar absorption coefficient of 6600 M^{-1} cm^{-1} at 260 nm.[79]

Absorption titration experiments were carried out by varying the concentration of the CT DNA while keeping the oxovanadium(IV) complex concentration constant. Due correction was made for the absorbance of CT DNA itself. Each spectrum was recorded after equilibration for 5 min. The intrinsic equilibrium binding constant (K_b) and the binding site size (s) of the complexes **1**–**4** to CT DNA were obtained by McGhee–von Hippel (MvH) method using the expression of Bard and co-workers by monitoring the change in the absorption intensity of the spectral bands with increasing concentration of CT DNA by regression analysis using Equation (1),

$$(\varepsilon_a - \varepsilon_f)/(\varepsilon_b - \varepsilon_f) = \{b - (b^2 - 2K_b^2C_t[DNA]_t/s)^{1/2}\}/2K_bC_t \ \ldots \quad (1)$$

where $b = 1 + K_bC_t + K_b[DNA]_t/2s$, ε_a is the extinction coefficient observed for the absorption band at a given DNA concentration, ε_f is the extinction coefficient of the complex free in solution, ε_b is the extinction coefficient of the complex when fully bound to DNA, K_b is the equilibrium binding constant, C_t is the total metal complex concentration, $[DNA]_t$ is the DNA concentration in nucleotides and s is the binding site size in base pairs.[80,81] The nonlinear least-squares analysis was done using Origin Lab, version 8.0.

DNA melting experiments were carried out by monitoring the absorption intensity of CT DNA (150 μM) at 260 nm at various temperatures, both in the absence and presence of the oxovanadium(IV) complexes (15 μM). Measurements were carried out using a Perkin–Elmer Lambda 35 spectrophotometer equipped with a Peltier temperature-controlling programmer (PTP 6) (±0.1 °C) on increasing the temperature of the solution by 0.5 °C per min.

Viscometric titrations were performed with a Schott AVS 310 Automated Viscometer. The viscometer was thermostatted at 37 °C in a constant temperature bath. The initial concentration of CT DNA was 140 μM in NP (nucleotide pair) and the flow times were measured with an automated timer. Each reading was taken on addition of 100 μL of complex stock solution of 200 μM. Each sample was measured 3 times and an average flow time was calculated. Data were presented as $(\eta/\eta_0)^{1/3}$ vs. [complex]/[DNA], where η is the viscosity of DNA in the presence of the complex and η_0 is that of DNA alone. Viscosity values were calculated from the observed flow time of DNA-containing solutions (t) corrected for that of the buffer alone (t_0), $\eta = (t - t_0)/t_0$.

DNA Cleavage Study: The cleavage of supercoiled (SC) pUC19 DNA (30 μM, 0.2 μg, 2686 base pairs) was studied by agarose gel electrophoresis using metal complexes in 50 mM Tris-HCl buffer (pH 7.2) containing 50 mM NaCl and 1.5% DMF. The photo-induced DNA cleavage reactions were carried out under illuminated conditions using UV-A light of 365 nm (6 W, Model LF-206.LS Bangalore Genei) or diode laser light of 785 nm (Model: LQC785–100C, Newport Corporation, LD module, continuous-wave circular beam). The laser power was 100 mW, measured using Spectra Physics CW Laser Power Meter (Model 407A). After light exposure, each sample was incubated for 1.0 h at 37 °C and analyzed for the photo-cleaved products using gel electrophoresis. The mechanistic studies were carried out using different additives (NaN_3, 0.5 mM; TEMP, 0.5 mM; DABCO, 0.5 mM; DMSO, 6 μL; KI, 0.5 mM; catalase, 4 units; SOD, 4 units) prior to the addition of the complex. For the D_2O experiment, this solvent was used for dilution of the

sample to 20 μL final volume. The samples after incubation in a dark chamber were added to the loading buffer containing 0.25% bromophenol blue, 0.25% xylene cyanol, 30% glycerol (3 μL) and the solution was finally loaded on 1% agarose gel containing 1.0 μg/mL ethidium bromide. Electrophoresis was carried out in a dark room for 1.0 h at 75 V in TAE (Tris-acetate EDTA) buffer. Bands were visualized by UV light and photographed. The extent of SC DNA cleavage was measured from the intensities of the bands using UVITEC Gel Documentation System. Due corrections were made for the low level of nicked circular (NC) form of DNA present in the original SC DNA sample and for the low affinity of EB binding to SC compared to NC and linear forms of DNA.[82] The concentrations of the complexes and additives corresponded to that in the 20 μL final volume of the sample using Tris buffer. The observed error in measuring the band intensities was about 5%.

Cell Cytotoxicity Assay: The photocytotoxicity of the complexes **1**–**4** were studied using 3-(4,5-dimethylthiazol-2-yl)-2,5-diphenyltetrazolium bromide (MTT) assay which is based on the ability of mitochondrial dehydrogenases of viable cells to cleave the tetrazolium rings of MTT forming dark purple membrane-impermeable crystals of formazan that could be quantified spectroscopically in DMSO.[83] About 10,000 human cervical cancer HeLa cells were plated in 96 wells culture plate in Dulbecco's Modified Eagle Medium (DMEM) containing 10% FBS. After 24 h of incubation at 37 °C in a CO_2 incubator, complexes with various concentrations in 1% DMSO were added to the cells and incubation was continued for 3 h in dark. The medium was subsequently replaced with PBS and photo-irradiation was done in visible light (400–700 nm) using a Luzchem Photoreactor (Model LZC-1, Ontario, Canada) fitted with Sylvania make 8 fluorescent white tubes with a fluence rate of 2.4 mW cm^{-2} to provide a total light dose of 10 *J* cm^{-2}. After photoexposure, PBS was removed and replaced with DMEM-FBS and incubation was continued for further period of 12 h in dark. After this incubation period, a 25 μ*L* of 4 mg per mL of MTT was added to each well and incubation was done for an additional period of 3 h. The culture medium was finally discarded and 200 μ*L* of DMSO was added to dissolve the formazan crystals and the absorbance at 595 nm was determined using a BIORAD ELISA plate reader. Cytotoxicity of the complexes was measured as the percentage ratio of the absorbance of the treated cells to the untreated controls. The IC_{50} values were determined by nonlinear regression analysis (GraphPad Prism).[30]

DAPI Staining: 4′,6-Diamidino-2-phenylindole (DAPI) staining was carried out to monitor the changes in nuclear morphology and chromatin organization following photoexposure after treatment with the py-tpy complex **4** using reported procedures.[84] Briefly, the control and the cells were treated with complex **4** (15 μM) for 4 h in dark followed by irradiation with visible light of 400–700 nm (10 *J* cm^{-2}). After 2 h incubation in fresh media the samples were fixed with 3.7% (v/v) paraformaldehyde in PBS for 10 min at room temperature. The fixed cells were then permeabilized with TBST [50 mM Tris-HCl (pH 7.4), 150 mM NaCl, and 0.1% Triton X-100] for 5 min and then stained with DAPI (10 μg mL^{-1} in PBS) for 5 min. The cells after being washed thrice with PBS were examined under a fluorescence microscope (Leica DM IL microscope with integrated Leica DFC 320 R2 camera and IL50 image software) with 360/40 nm excitation and 460/50 nm emission filters. The live cells were identified by essentially no or very low nuclear staining and the cell morphology. The apoptotic cells that uptake DAPI were identified by the presence of highly condensed or fragmented nuclei with significant alteration in cell morphology.

Fluorescence Imaging: To study the uptake behavior of the complexes, live cell imaging experiments were carried out.[85,86] HeLa cancer cells were grown on 30 mm tissue culture dish in DMEM/10% FBS for 24 h in a CO_2 incubator at 37 °C with 5% CO_2 until the cells attained 60% confluency. Thereafter, the compounds (the ligands and the complexes) dissolved in DMSO were added to the cells in dark so as to give a final compound concentration of 100 μM and DMSO concentration of 1% in the culture media. The cells were incubated for 4 h in a CO_2 incubator in dark and the culture media containing the compounds were discarded. The cells were washed with phosphate buffered saline and fresh DMEM/10% FBS was added to the cells which were then observed using the LUCPLFLN 20X objective of a fluorescence microscope (Olympus IX-71) with 360 nm excitation and 460 nm emission. The images were acquired using Olympus DP71 camera and the images were processed using Image Pro-Express 6.0 software. The exposure time for the fluorescence images was 500 ms with a gain of 4 units. The bright field images were acquired at an exposure time of 100 ms with a gain of 2 units.[87]

Supporting Information (see footnote on the first page of this article): Experimental details on DNA binding, cleavage and MTT assay. Figures S1–S4: ESI-MS spectra, Figure S5: emission spectra, Figure S6: cyclic voltammetric responses, Figure S7: unit cell packing diagram of **1**·1.5ClO_4·0.5PF_6·CH_3CN, Figure S8: DNA binding plots, Figure S9–S11: gel electrophoresis diagrams, Figure S12: MTT assay plots, Table S1: bonding parameters, Table S2: statistical analysis data.

Acknowledgments

We thank the Department of Science and Technology (DST), Government of India for financial support (SR/S5/MBD-02/2007). B. B. thanks the Council of Scientific and Industrial Research, New Delhi, for a fellowship. A. R. C. thanks DST for a J. C. Bose Fellowship. We also thank the Alexander von Humboldt Foundation, Germany, for donation of an electroanalytical system.

[1] D. S. Sigman, A. Mazumder, D. M. Perrin, *Chem. Rev.* **1993**, *93*, 2295–2316.
[2] A. E. Friedman, J. C. Chambron, J. P. Sauvage, N. J. Turro, J. K. Barton, *J. Am. Chem. Soc.* **1990**, *112*, 4960–4962.
[3] P. U. Maheswari, M. Palaniandavar, *J. Inorg. Biochem.* **2004**, *98*, 219–230.
[4] J. K. Barton, A. T. Danishefsky, J. M. Goldberg, *J. Am. Chem. Soc.* **1984**, *106*, 2172–2176.
[5] H. Y. Mei, J. K. Barton, *Proc. Natl. Acad. Sci. USA* **1988**, *85*, 1339–1343.
[6] A. D. Guerzo, A. K. D. Mesmaeker, M. Demeunynck, J. Lhomme, *J. Chem. Soc., Dalton Trans.* **2000**, 1173–1180.
[7] K. E. Erkkila, D. T. Odom, J. K. Barton, *Chem. Rev.* **1999**, *99*, 2777–2796.
[8] C. Metcalfe, J. A. Thomas, *Chem. Soc. Rev.* **2003**, *32*, 215–224.
[9] S. Arounaguiri, B. G. Maiya, *Inorg. Chem.* **1999**, *38*, 842–843.
[10] Q. L. Zhang, J. G. Liu, J. Z. Liu, H. Li, Y. Yang, H. Xu, H. Chao, L. N. Ji, *Inorg. Chim. Acta* **2002**, *339*, 34–40.
[11] Q. L. Zhang, J. H. Liu, J. Z. Liu, P. X. Zhang, X. Z. Ren, Y. Liu, Y. Huang, L. N. Ji, *J. Inorg. Biochem.* **2004**, *98*, 1405–1412.
[12] A. M. Angeles-Boza, P. M. Bradley, P. K. L. Fu, S. E. Wicke, J. Bacsa, K. R. Dunbar, C. Turro, *Inorg. Chem.* **2004**, *43*, 8510–8519.
[13] B. Armitage, *Chem. Rev.* **1998**, *98*, 1171–1200.

[14] F. S. Mackay, J. A. Woods, P. Heringová, J. Kašpárková, A. M. Pizarro, S. A. Moggach, S. Parsons, V. Brabec, P. J. Sadler, *Proc. Natl. Acad. Sci. USA* **2007**, *104*, 20743–20748.
[15] A. M. Angeles-Boza, H. T. Chifotides, J. D. Aguirre, A. Chouai, P. K.-L. Fu, K. R. Dunbar, C. Turro, *J. Med. Chem.* **2006**, *49*, 6841–6947.
[16] M. J. Rose, N. L. Fry, R. Marlow, L. Hinck, P. K. Mascharak, *J. Am. Chem. Soc.* **2008**, *130*, 8834–8846.
[17] L. J. K. Boerner, J. M. Zaleski, *Curr. Opin. Chem. Biol.* **2005**, *9*, 135–144.
[18] U. Schatzschneider, *Eur. J. Inorg. Chem.* **2010**, 1451–1467.
[19] N. J. Farrer, L. Salassa, P. J. Sadler, *Dalton Trans.* **2009**, 10690–10701.
[20] A. D. Ostrowski, P. C. Ford, *Dalton Trans.* **2009**, 10660–10669.
[21] H. T. Chifotides, K. R. Dunbar, *Acc. Chem. Res.* **2005**, *38*, 146–156.
[22] R. Bonnett, *Chemical Aspects of Photodynamic Therapy*, Gordon & Breach, London, UK, **2000**.
[23] W.-H. Wei, Z. Wang, T. Mizuno, C. Cortez, L. Fu, M. Sirisawad, L. Naumovski, D. Magda, J. L. Sessler, *Dalton Trans.* **2006**, 1934–1942.
[24] S. Atilgan, Z. Ekmeckci, A. L. Dogan, D. Guc, E. U. Akkaya, *Chem. Commun.* **2006**, 4398–4400.
[25] J. Mao, Y. Zhang, J. Zhu, C. Zhang, Z. Guo, *Chem. Commun.* **2009**, 908–910.
[26] J. L. Sessler, G. Hemmi, T. D. Mody, T. Murai, A. Burrell, S. W. Young, *Acc. Chem. Res.* **1994**, *27*, 43–50.
[27] M. Ochsner, *J. Photochem. Photobiol.* **1996**, *B32*, 3–9.
[28] S. I. Moriwaki, J. Misawa, Y. Yoshinari, I. Yamada, M. Takigawa, Y. Tokura, *Photodermatol. Photoimmunol. Photomed.* **2001**, *17*, 241–243.
[29] P. K. Sasmal, S. Saha, R. Majumdar, R. R. Dighe, A. R. Chakravarty, *Chem. Commun.* **2009**, 1703–1705.
[30] S. Saha, R. Majumdar, M. Roy, R. R. Dighe, A. R. Chakravarty, *Inorg. Chem.* **2009**, *48*, 2652–2663.
[31] C. J. Burrows, J. G. Muller, *Chem. Rev.* **1998**, *98*, 1109–1151.
[32] K. Szacilowski, W. Macyk, A. Drzewiecka-Matuszek, M. Brindell, G. Stochel, *Chem. Rev.* **2005**, *105*, 2647–2694.
[33] K. H. Thompson, C. Orvig, *Coord. Chem. Rev.* **2001**, *219–221*, 1033–1053.
[34] A. S. Tracey, G. R. Willsky, E. S. Takeuchi, in: *Vanadium: Chemistry, Biochemistry Pharmacology and Practical Applications*, CRC Press, Taylor and Francis Group, Boca Raton, **2007**.
[35] F. Van de Velde, I. W. Arends, R. A. Sheldon, *J. Inorg. Biochem.* **2000**, *80*, 81–89.
[36] J. M. Winter, B. S. Moore, *J. Biol. Chem.* **2009**, *284*, 18577–18581.
[37] J. Liang, M. Madden, V. K. Shah, R. H. Burris, *Biochemistry* **1990**, *29*, 8577–8581.
[38] K. M. Walton, J. E. Dixon, *Annu. Rev. Biochem.* **1993**, *62*, 101–120.
[39] J. K. Klarlund, *Cell* **1985**, *41*, 707–717.
[40] P. J. Stankiewicz, A. S. O. Tracey, in: *Metal Ions in Biological Systems* (Eds.: H. Sigel, A. Sigel), Dekker, New York, **1995**, vol. 31, pp. 249–285.
[41] D. C. Crans, A. S. Tracey, in: *Vanadium Compounds: Chemistry, Biochemistry and Therapeutic Applications* (Eds.: A. S. Tracey, D. C. Crans), American Chemical Society, Washington, DC, **1998**, vol. 711, pp. 2–29.
[42] D. Rehder, J. C. Pessoa, C. F. G. C. Geraldes, M. M. C. A. Castro, T. Kabanos, T. Kiss, B. Meier, G. Micera, L. Pettersson, M. Rangel, A. Salifoglou, I. Turel, D. Wang, *J. Biol. Inorg. Chem.* **2002**, *7*, 384–396.
[43] J. Kuwahara, T. Suzuki, Y. Sugiura, *Biochem. Biophys. Res. Commun.* **1985**, *129*, 368–374.
[44] H. Sakurai, H. Tamura, K. Okatani, *Biochem. Biophys. Res. Commun.* **1995**, *206*, 133–137.
[45] K. Toshima, R. Takano, T. Ozawa, S. Matsumura, *Chem. Commun.* **2002**, 212–213.
[46] J.-P. Collin, S. Guillerez, J.-P. Sauvage, F. BarigeUetti, L. D. CoIa, L. Flamigni, V. Balzanil, *Inorg. Chem.* **1992**, *31*, 4112–4117.
[47] K. Becker, C. Herold-Mende, J. J. Park, G. Lowe, R. H. Schirmer, *J. Med. Chem.* **2001**, *44*, 2784–2792.
[48] C. Yu, K. H.-Y. Chan, K. M.-C. Wong, V. W.-W. Yam, *Chem. Commun.* **2009**, 3756–3758.
[49] F. Guo, W. Sun, *J. Phys. Chem. B* **2006**, *110*, 15029–15036.
[50] S. Roy, S. Saha, R. Majumdar, R. R. Dighe, A. R. Chakravarty, *Polyhedron* **2010**, *29*, 3251–3256.
[51] R. B. Nair, E. S. Tang, S. L. Kirkland, C. J. Murphy, *Inorg. Chem.* **1998**, *37*, 139–141.
[52] P. Shi, Q. Jiang, Y. Zhao, Y. Zhang, J. Lin, L. Lin, J. Ding, Z. Guo, *J. Biol. Inorg. Chem.* **2006**, *11*, 745–752.
[53] S. Moghaddas, P. Hendry, R. J. Geue, C. Qin, A. M. T. Bygott, A. M. Sargeson, N. E. Dixon, *J. Chem. Soc., Dalton Trans.* **2000**, 2085–2089.
[54] H. C. Becker, B. Norden, *J. Am. Chem. Soc.* **1999**, *121*, 11947–11952.
[55] C. V. Kumar, E. H. Asuncion, *J. Am. Chem. Soc.* **1993**, *115*, 8541–8553.
[56] L. E. Gunther, A. S. Yong, *J. Am. Chem. Soc.* **1968**, *90*, 7323–7328.
[57] J. M. Veal, R. L. Rill, *Biochemistry* **1991**, *30*, 1132–1140.
[58] G. Cohen, H. Eisenberg, *Biopolymers* **1969**, *8*, 45–55.
[59] T. Otieno, M. R. Bond, L. M. Mokry, R. B. Walter, C. J. Carrano, *Chem. Commun.* **1996**, 37–38.
[60] D. W. J. Kwong, O. Y. Chan, R. N. S. Wong, S. M. Musser, L. Vaca, S. I. Chan, *Inorg. Chem.* **1997**, *36*, 1276–1277.
[61] A. U. Khan, *J. Phys. Chem.* **1976**, *80*, 2219–2227.
[62] P. B. Merkel, D. R. Kearns, *J. Am. Chem. Soc.* **1972**, *94*, 1029–1030.
[63] S. Dhar, D. Senapati, P. A. N. Reddy, P. K. Das, A. R. Chakravarty, *Chem. Commun.* **2003**, 2452–2453.
[64] R. M. Burger, *Chem. Rev.* **1998**, *98*, 1153–1170.
[65] S. E. Wolkenberg, D. L. Boger, *Chem. Rev.* **2002**, *102*, 2477–2496.
[66] H. C. Kang, I.-J. Kim, H.-W. Park, S.-G. Jang, S.-A. Ahn, S. N. Yoon, H. J. Chang, B. C. Yoo, J.-G. Park, *Cancer Lett.* **2007**, *247*, 40–47.
[67] E. Delaey, F. V. Laar, D. De Vos, A. Kamuhabwa, P. Jacobs, P. De Witte, *J. Photochem. Photobiol.* **2000**, *B55*, 27–36.
[68] H. J. Motulsky, in: *Analyzing Data with GraphPad Prism*, GraphPad Software Inc., San Diego, CA, **1999**.
[69] D. D. Perrin, W. L. F. Armarego, D. R. Perrin, in: *Purification of Laboratory Chemicals*, Pergamon Press, Oxford, **1980**.
[70] J. G. Collins, A. D. Sleeman, J. R. Aldrich-Wright, I. Greguric, T. W. Hambley, *Inorg. Chem.* **1998**, *37*, 3133–3141.
[71] E. Amouyal, A. Homsi, J.-C. Chambron, J.-P. Sauvage, *J. Chem. Soc., Dalton Trans.* **1990**, 1841–1845.
[72] S. A. Moya, R. Pastene, H. L. Bozec, P. J. Baricelli, A. J. Pardey, J. Gimeno, *Inorg. Chim. Acta* **2001**, *312*, 7–14.
[73] G. Albano, V. Balzani, E. C. Constable, M. Maestri, D. R. Smith, *Inorg. Chim. Acta* **1998**, *277*, 225–231.
[74] X. Peng, Y. Xu, S. Sun, Y. Wu, J. Fan, *Org. Biomol. Chem.* **2007**, *5*, 226–228.
[75] O. Kahn, in: *Molecular Magnetism*, VCH, Weinheim, Germany, **1993**.
[76] N. Walker, D. Stuart, *Acta Crystallogr., Sect. A: Found. Crystallogr.* **1983**, *39*, 158–166.
[77] G. M. Sheldrick, *SHELX-97*, *Programs for Crystal Structure Solution and Refinement*, University of Göttingen, Göttingen, Germany, **1997**.
[78] C. K. Johnson, *ORTEP*, *Report ORNL-5138*, Oak Ridge National Laboratory, Oak Ridge, TN, **1976**.
[79] S. P. Foxon, C. Metcalfe, H. Adams, M. Webb, J. A. Thomas, *Inorg. Chem.* **2007**, *46*, 409–416.
[80] J. D. McGhee, P. H. von Hippel, *J. Mol. Biol.* **1974**, *86*, 469–489.

[81] M. T. Carter, M. Rodriguez, A. J. Bard, *J. Am. Chem. Soc.* **1989**, *111*, 8901–8911.
[82] J. Bernadou, G. Pratviel, F. Bennis, M. Girardet, B. Meunier, *Biochemistry* **1989**, *28*, 7268–7275.
[83] T. Mosmann, *J. Immunol. Methods* **1983**, *65*, 55–63.
[84] S. Park, S. P. Hong, T. Y. Oh, S. Bang, J. B. Chung, S. Y. Song, *Photochem. Photobiol. Sci.* **2008**, *7*, 769–774.
[85] J. Farrera-Sinfreu, E. Giralt, S. Castel, F. Albericio, M. Royo, *J. Am. Chem. Soc.* **2005**, *127*, 9459–9468.
[86] M. M. Pires, J. Chmielewski, *Org. Lett.* **2008**, *10*, 837–840.
[87] A. Füssl, A. Schleifenbaum, M. Göritz, A. Riddell, C. Schultz, R. Krämer, *J. Am. Chem. Soc.* **2006**, *128*, 5986–5987.

Received: October 15, 2010
Published Online: February 4, 2011

